nature communications

Article

https://doi.org/10.1038/s41467-025-57848-w

# Foxa2-dependent uterine glandular cell differentiation is essential for successful implantation

Received: 13 September 2024

Accepted: 5 March 2025

Published online: 12 March 2025

Check for updates

Zhaoyu Jia[1,5], Bo Li[2,3,5], Mitsunori Matsuo[2,3,4], Amanda Dewar[2,3], Anxhela Mustafaraj[2,3], Sudhansu K. Dey[2,3] ✉, Jia Yuan[1] ✉ & Xiaofei Sun[2,3] ✉

Uterine receptivity is essential for successful implantation. In mice, uterine receptivity begins with the secretion of LIF from uterine glands stimulated by estrogen on the morning of day 4 pregnancy. We hypothesize that gland readiness for estrogen stimulation is indispensable for uterine receptivity. The current study reveals that uterine glands undergo a differentiation process with expanded branching during the preimplantation period. The single-cell RNA profiling of glandular cells identifies that LIF is expressed exclusively in a *Prss29*+ subgroup of glandular cells on day 4 of pregnancy. Interestingly, *Foxa2*-deficient glands lacking LIF production fail to develop branches and the functional *Prss29*+ subgroup. This *Prss29*+ subgroup develops prior to estrogen secretion. Collectively, our findings show that uterine glands undergo a FOXA2-dependent maturation process to acquire the competence, named "transitional phase", for entering the receptive phase. The "transitional phase", predicting uterine receptivity one day before implantation, is a landmark concept in uterine receptivity.

Uterine glands play a critical role in uterine receptivity. Uterine receptivity, along with an implantation-competent blastocyst, is a prerequisite for successful implantation[1,2]. In mice, the uterus becomes receptive for a limited period on day 4 of pregnancy (day 1 = vaginal plug), initiated by estrogen secretion in the morning of day 4. Leukemia inhibitory factor (*Lif*), an estrogen-responsive gene[3], is critical for uterine receptivity and implantation[4]. *Lif* is expressed in mouse uterine luminal epithelium on day 1 and specifically in uterine glands on day 4 of pregnancy[5]. In the absence of day 4 estrogen, LIF injection is sufficient to induce implantation[6]. Additionally, LIF is also restricted to the human endometrial glands during the secretory phase[7], and lower levels of LIF are correlated with unexplained infertility[8].

Recent studies demonstrated that Forkhead box a2 (FOXA2) is essential for LIF production prior to implantation. FOXA2, a member of the FoxA family of transcription factors, plays a crucial role in the development of various organs and biological functions[9]. In both mouse and human uteri, FOXA2 is expressed in glandular epithelial cells[10,11]. Female mice with uterine epithelial deletion (*Foxa2*$^{f/f}$ *Ltf*$^{Cre/+}$) of *Foxa2* are infertile due to LIF deficiency[11,12]. Our recent study showed that a deficiency of *Foxa2* in uterine glands leads to embryonic diapause[13]. However, the precise mechanism through which FOXA2 regulates LIF expression in uterine glands is still unknown.

Despite the critical role of uterine glands during pregnancy[14], our understanding of glandular morphology and function remains limited. The three-dimensional structure of uterine glands was only recently elucidated[15]. In contrast, the structure of glands in another female reproductive organ, the mammary gland, has been recognized for years. Typically, the mammary epithelium consists of a few small ducts

[1]Advanced Medical Research Institute, Cheeloo College of Medicine, Shandong University, Jinan, Shandong, China. [2]Reproductive Sciences Center, Division of Developmental Biology, Cincinnati Children's Hospital Medical Center, Cincinnati, OH, USA. [3]College of Medicine, University of Cincinnati, Cincinnati, OH, USA. [4]Present address: Department of Obstetrics and Gynecology, University of Tokyo, Tokyo, Japan. [5]These authors contributed equally: Zhaoyu Jia, Bo Li ✉e-mail: sk.dey@cchmc.org; Jia.Yuan@sdu.edu.cn; Xiaofei.sun@cchmc.org

at birth, and branching morphogenesis shapes a ductal tree during puberty. At the beginning of pregnancy, mammary glands proliferate rapidly and undergo side branching, and the glandular cells become highly differentiated during lactation to produce milk[16]. Since both the uterus and the mammary gland are under the control of ovarian hormones, the changes in mammary gland structure and function during pregnancy led us to presume that uterine glands also undergo functional differentiation.

In our study of FOXA2's role in embryonic diapause, we noticed that *Foxa2*$^{f/f}$ *Ltf*$^{Cre/+}$ uterine glands exhibited significantly reduced branching, prompting our hypothesis that FOXA2 plays roles in glandular morphology and function. Therefore, we systematically studied the morphological changes in uterine glands during the preimplantation period and analyzed uterine glandular cells at the single-cell level prior to implantation. We found that uterine glands undergo side-branching and cell differentiation during the preimplantation period, and this differentiation is indispensable for LIF secretion and subsequent successful implantation. Our findings add a new dimension to the definition of uterine receptivity, emphasizing the importance of uterine gland maturation alongside luminal epithelial readiness for the homing of implantation-competent embryos at the blastocyst stage. Our current study suggests that uterine glands need to undergo a pre-implantation maturation process to initiate successful implantation, which is dependent on FOXA2 via LIF.

## Results

### Uterine epithelial deficiency of *Foxa2* disrupts normal gland morphology before implantation

The uterine epithelial-specific deletion of *Foxa2* disrupts LIF production, causing implantation failure[11]. However, the mechanism by which FOXA2 regulates LIF production remains unclear. Previously, we showed that embryos enter diapause in *Foxa2*$^{f/f}$ *Ltf*$^{Cre/+}$ uteri[13], in which *Foxa2* is deleted during puberty. While studying the uterine lumen structures using three-dimensional imaging techniques[15], we found that *Foxa2*$^{f/f}$ *Ltf*$^{Cre/+}$ glands exhibit different morphological structures compared to *Foxa2*$^{f/f}$ *Ltf*$^{+/+}$ glands on day 4 of pregnancy. Most *Foxa2*$^{f/f}$*Ltf*$^{+/+}$ glands have more than one branch coiled at the ends, while the number of branches of *Foxa2*$^{f/f}$ *Ltf*$^{Cre/+}$ glands is significantly decreased, with many glands having no branches at all (Fig. 1a, c). The number of branches is defined in the scheme shown in Fig. 1b. The diameter of the *Foxa2*$^{f/f}$ *Ltf*$^{Cre/+}$ glands is larger than that of *Foxa2*$^{f/f}$ *Ltf*$^{+/+}$ glands (Fig. 1d).

To investigate whether this defect is due to gland development before pregnancy, we also examined uterine epithelial structures before puberty on postnatal day 30. Since *Cre* driven by *Ltf* promoter is not active before puberty[17], the glandular morphology is similar in both *Foxa2*$^{f/f}$ *Ltf*$^{+/+}$ and *Foxa2*$^{f/f}$*Ltf*$^{Cre/+}$ uteri. The glands are shorter and composed mostly of primary ducts with limited branches (Supplementary Fig. 1a, b). To examine whether *Foxa2*$^{f/f}$ *Ltf*$^{Cre/+}$ gland morphology is abnormal in mature females before pregnancy, we examined uterine epithelial structures in *Foxa2*$^{f/f}$ *Ltf*$^{+/+}$ and *Foxa2*$^{f/f}$*Ltf*$^{Cre/+}$ females during diestrus at around 7 weeks old. Similar to the day 4 data, the number of branches of *Foxa2*$^{f/f}$ *Ltf*$^{Cre/+}$ glands is significantly decreased (Supplementary Fig. 1c, d). Interestingly, *Foxa2*$^{f/f}$ *Ltf*$^{+/+}$ glands during diestrus have fewer branches than those on day 4 of pregnancy. For example, the percentages of glands with more than 1 branch are ~60% during diestrus and ~80% on day 4 of pregnancy (Fig. 1c and Supplementary Fig. 1d). These results show that uterine glands undergo dynamic changes through estrous cycles and early pregnancy, and the branching activity depends on glandular FOXA2.

### The morphology of uterine glands undergoes dynamic changes during the preimplantation of pregnancy

In mice, uterine luminal epithelia undergo drastic changes to enter the receptive phase: on day 1 of pregnancy, luminal epithelia show hypertrophy under the influence of estrogen, whereas by day 4 of pregnancy, they shrink to a slit-like structure with a closed lumen cavity[18]. However, the changes in glandular structure during the preimplantation stage have not been clearly investigated, despite the key role of uterine glands in implantation[19]. To further profile the morphological changes of uterine glands in early pregnancy, we investigated uterine epithelial structure across all four preimplantation days using recently developed tissue clearing and 3D imaging techniques. As expected, uterine lumen folding reduces from day 1 to day 4 of pregnancy. Glands are pushed among the lumen folding due to the expansion of the lumen on day 1 of pregnancy (Fig. 1e). Usually, multiple glands cluster together, with about 70% of the glands having 0 or 1 branches (Fig. 1e, f). By day 2 of pregnancy, the number of glands with more than 1 branch increases, while the diameter of the uterine horn sharply decreases. Most branches are still very short and resemble grape clusters. Following further extension of uterine glands on day 3, the primary gland ducts become more prominent on day 4 of pregnancy. At this time, more than 80% of glands have more than 1 branch, and the branches are more distinct from the primary ducts owing to branch extension. In summary, uterine glands extend and develop branches before implantation.

### Uterine glandular epithelial cells show heterogeneity on day 4 of pregnancy

Our observations of the glandular morphological changes in the first 4 days of pregnancy prompt the question whether the development of uterine glandular branches indicates glandular cell differentiation during the preimplantation period. The single cell RNAseq (scRNAseq) experiment is of great help in categorizing cell populations. In a previous scRNAseq study of mouse uterine cells on day 4 of pregnancy[20], around 15% of total cells were identified as glandular cells (~900 cells), whereas 52% cells were stromal cells (~3100 cells). The low percentage and cell number undermined further sub-clustering of glandular cells. To boost the glandular cell numbers, we crossed Rosa26-tdTomato reporter mice with Ltf-Cre mice to establish a mouse line (*Rosa26*$^{tdTomato}$*Ltf*$^{Cre/+}$) with all uterine epithelial cells labeled with tomato proteins (Supplementary Fig. 2a). To prepare cells for sequencing, luminal epithelial cells were first isolated using pancreatin and dispase on day 4 of pregnancy. The remaining uterine tissue, including glands, was further digested into single cells except for cells in muscle layers. Glandular cells were sorted out via tomato signals using flow cytometry (Supplementary Fig. 2b). The sorted glandular cells were pooled from multiple uterine samples ($N = 8$) and mixed with other endometrial single cell suspension from 4 females. The mixture of cells with an increased proportion of glandular cells was subjected to further scRNAseq analysis (Fig. 2a).

A total of 25,839 cells passed the initial quality control. There were a total of 19 distinct clusters identified in day 4 uteri endometrium, including three luminal epithelial cells (LE), four glandular epithelial cells (GE), two stromal cells (Str), two pericytes (Peri), three endothelial cells (Endo), two mesothelial cells (Meso), granulocytes (Gran), macrophages (Mac), and T cells (T), as labeled by different marker genes (Fig. 2b–d). *Epcam* was highly expressed in all epithelial cells. *Foxa2* was enriched in GE populations, whereas *Wnt7a* was enriched in LE populations but not in GEs (Fig. 2e). Of note, four GE groups contained a total of 9154 cells (~35.4% of all sequenced cells), allowing us to study different subpopulations of GEs (Fig. 2f). Most of the sequenced cells accumulated at the G2/M phase of cell cycles (Supplementary Fig. 3a). A portion of granulocytes appeared at the G1 phase, whereas a cluster of cells in GE_1 was at the S phase. The expression of Tomato RNA in epithelial cells is confirmed in Supplementary Fig. 3b.

### Characteristics of glandular epithelial cells in mouse uteri on day 4

The expression of C-X-C motif ligand 15 (*Cxcl15*) separates GE populations from other uterine cells (Fig. 3a). *Mki67* and H2A clustered

https://doi.org/10.1038/s41467-025-57848-w

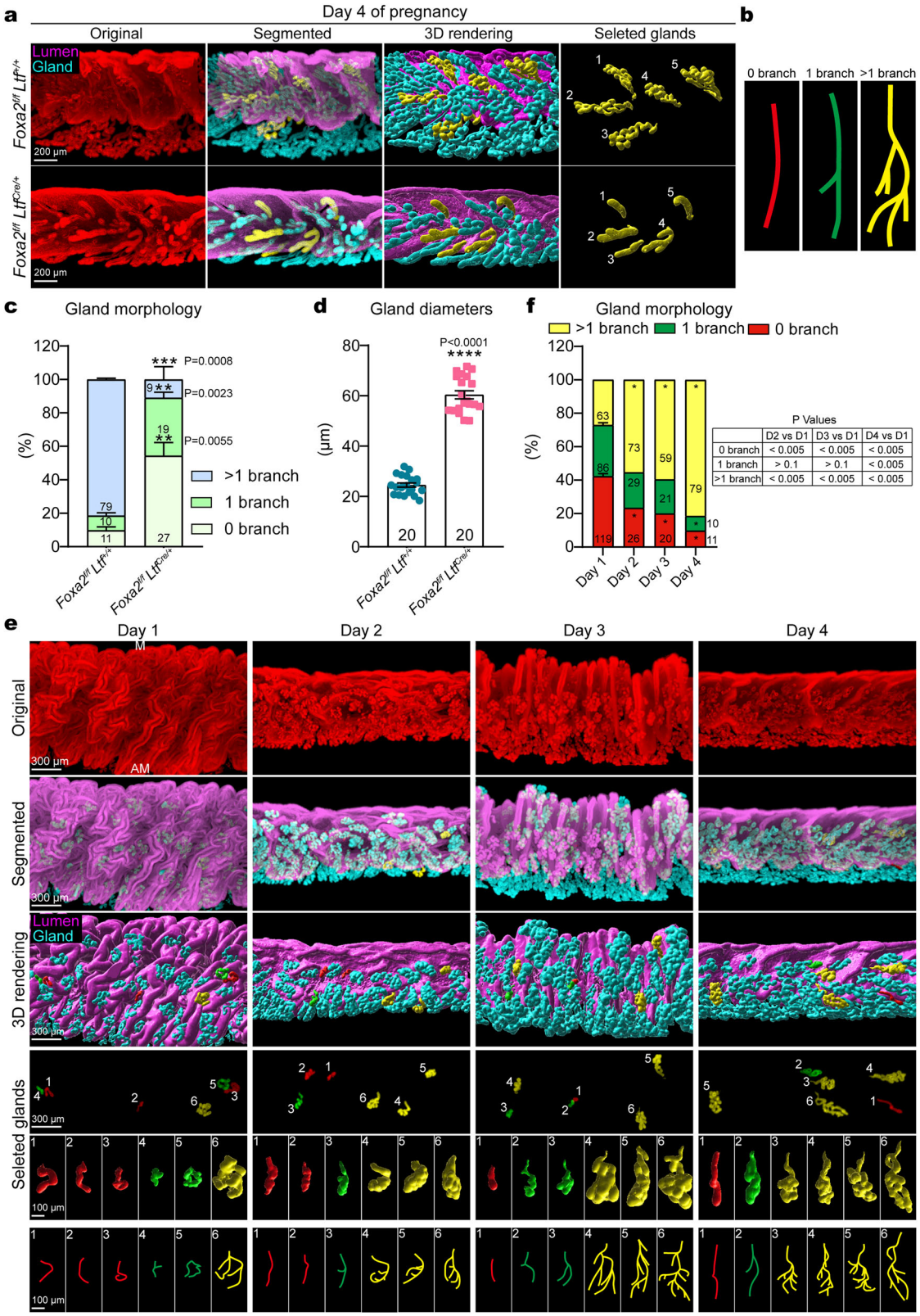


histone 24 (*H2ac24*) positive cells are concentrated in the GE_1 group, suggesting its high cell proliferation potential. Interestingly, *Foxj1*, a marker of ciliated cells, is enriched in GE_2 cells, indicating their role in moving lumen contents. Serine peptidase inhibitor Kazal type 1 (*Spink1*) is expressed in GE_3 and GE_4 groups. Notably, *Lif* is solely expressed in GE_4, indicating GE_4's critical role in implantation (Fig. 3a, b). To further investigate the functions of glandular populations, KEGG and GO gene function enrichment analysis were performed using the expression profiles in 4 GE groups. These enrichment analyses show that cell cycle, DNA replication, and RNA splicing genes are enriched in GE_1; GE_2 has abundant genes in WNT signaling pathway, gland development, and cilium organization. GE_3 shows high fatty acid and lipid metabolic activity, including glutathione and sphingolipid metabolism; GE_4 shows high protein processing and export activity (Fig. 3c, d). The expression levels of genes within the function groups of protein processing, gland development,

**Fig. 1 | Uterine epithelial deficiency of *Foxa2* disrupts normal glandular morphological development before implantation. a** 3D visualization of day 4 mouse uteri in *Foxa2*$^{f/f}$ *Ltf*$^{+/+}$ and *Foxa2*$^{f/f}$ *Ltf*$^{Cre/+}$ females. Original (staining of E-Cadherin), segmented, and 3D rendered images of day 4 uteri. Five randomly selected individual glands from each group are colored in yellow to present the morphology. Scale bars: 200 µm. **b** Schematic definition of gland classification. Glands are classified to 3 types: 0, 1, and >1 branch. **c** Quantification of gland morphology in *Foxa2*$^{f/f}$ *Ltf*$^{+/+}$ ($n = 3$ uterine horns from 3 independent mice) and *Foxa2*$^{f/f}$ *Ltf*$^{Cre/+}$ ($n = 3$ uterine horns from 3 independent mice) females using the criteria defined in panel (**b**). Data are represented as mean ± SEM. Source data are provided as a Source Data file. (two-tailed unpaired Student's *t* test with equal variance assumed) **d** Diameters of *Foxa2*$^{f/f}$ *Ltf*$^{+/+}$ ($n = 20$ glands from 3 independent mice) and *Foxa2*$^{f/f}$ *Ltf*$^{Cre/+}$ ($n = 20$ glands from 3 independent mice) glands on day 4 of pregnancy. Data points represent individual gland measurements. Source data are provided as a Source Data file. Statistical significance was assessed using two-tailed unpaired Student's *t* test with equal variance assumed (mean ± SEM). **e** 3D visualization of wild-type mouse uteri from days 1, 2, 3, and 4 of pregnancy. Selected glands are colored in red with 0 branch, green with 1 branch, and yellow with more than 1 branch. Scale bars: 100 and 300 µm. M mesometrial pole, AM antimesometrial pole. **f** Quantification of gland branches in wild-type females on days 1–4 of pregnancy. Glands are randomly selected from 3 uterine horns of 3 independent mice. Statistical significance was assessed using a *Chi*-square test (*$P < 0.005$). Source data are provided as a Source Data file.

and fatty acid metabolism are plotted in heatmaps (Fig. 3e). These results show versatile functions in different GE groups and that genes of protein export are enriched in GE_4.

## Glandular epithelium heterogeneity on day 4 of pregnancy

A bird's-eye view of transcription in 4 GE groups by the Pearson correlation analysis indicates a gradual transcriptional change following the order GE_1- GE_2- GE_3- GE_4, since GE_2 shows high similarity with GE_1 and GE_3 and GE_3 shows high similarity with GE_2 and GE_4 (Fig. 2d). All 4 GE groups are re-plotted according to their transcriptional profile similarity (Fig. 4a). *Mki67* was mainly expressed in the GE_1 group, *Lif* was primarily expressed in the GE_4 group, and *Lgr5* was enriched in GE_2 (Fig. 4b).

To better understand the glandular cell differentiation trajectory, we studied RNA velocity kinetics using scVelo and the gradual transcriptional changes using Slingshot in the 4 GE groups. The RNA kinetic analysis showed cell state transition from GE_1 to GE_4 (Fig. 4c). The analysis by Slingshot trajectory further confirmed the direction of population kinetics in glandular cells: GE cells initiated from the GE_1 group, transmitted through GE_2 and GE_3 stages, and ultimately differentiated to the GE_4 group (Fig. 4d).

Transcription factors (TFs) are pivotal in making cell fate decisions[21], and TFs' activities are reflected by their downstream target gene levels. Using pySCENIC python package, we predicted transcriptional activity of TFs in various GE groups via the expression levels of downstream target genes (Fig. 4e). Forkhead box M1 (*Foxm1*), a gene tightly involved in cell proliferation[22], is predicted to be active in the GE_1 group with high cell proliferation potential. This prediction is supported by *Foxm1*'s expression in GE_1 (Supplementary Fig. 3c). *Mxd3* and *Brca1*, involved in various cancers[23,24], are another two TFs with predicted high activity in GE_1 (Fig. 4e and Supplementary Fig. 3c). Downstream target genes of GATA binding protein 2 (*Gata2*), which is indispensable for implantation[25], are enriched in GE_2 cells. GE_3 cells show high activity of sterol regulatory element binding transcription factor 1 (*Srebf1*), which plays a role in lipid metabolism[26]. The activity of Forkhead box O1 (*Foxo1*), a critical transcription factor for both mouse and human pregnancy[27,28], is highly implicated in the GE_4 group. All these results coordinate well with the predicted functions in each glandular group. The GE_4 group has high protein secretion activity, indicating its critical role in embryo implantation. Indeed, *Lif* is predominantly expressed in GE_4 cells (Figs. 3a and 4b). We also identified *Prss29* and *Krt83* as GE_4 specific marker genes on day 4 (Fig. 4f). *Prss29* positive cells, present only in GE_4, highly overlap with *Lif*+ cells (Fig. 4f).

## Cell to cell communication in day 4 mouse uteri

LIF is not the only gland-secreted protein critical to pregnancy success. In the glandless mouse model with uterine deficiency of *Foxa2* (*Foxa2*$^{f/f}$*Pgr*$^{cre/+}$), LIF supplement on day 4 of pregnancy cannot support the pregnancy to full term, although implantation occurs[11], suggesting uterine glands have roles beyond embryo implantation throughout pregnancy. To explore the secreted proteins by glands and their target cells, we studied the cell-cell connections using CellChat. The GE cells send and receive various signals in a group dependent manner (Fig. 5a). All 4 GE groups actively send macrophage migration inhibitory (MIF) factors (Fig. 5b). GE_1 cells secreted phosphoprotein 1 (SPP1, also known as Osteopontin) signals, which are involved in cell proliferation, migration, and tissue remodeling[29]. GE_2 cells send KIT and hedgehog (HH) signals, which are critical to proper cell differentiation[30,31]. Interestingly, Kitl secreted by GE_2 cells target on the receptor tyrosine kinase cKit expressed on GE_4 (Supplementary Fig. 4a), which may play a role in GE_4 cell differentiation. Cells in GE_3 and GE_4 send calcitonin (CALCR) and IGF signals (Fig. 5b). All four GE groups express receptors for Midkine (MK) and pleiotrophin (PTN) signals, which have roles in mitogenicity and tissue regeneration[32]. GE_1 and GE_2 are highly responsive to BMP signaling, whereas the GE_4 group is responsive to KIT signaling (Fig. 5c).

LIF is mainly produced by the GE_4 group, which is located at the end of pseudo time differentiation trajectory, indicating proper glandular differentiation is critical for LIF production. To further explore other signals secreted by GE_4 cells, we analyzed the detailed signals sent by GE_4 and their target cell populations. Str_1 is predicted as a major target population of signals sent by GE_4, including *Ihh*, *Wnt5a*, and *Pdgfa* (Fig. 5d). LE cells are targets of the LIF signaling and tumor necrosis factor superfamily member 10 (TNFSF10), which triggers extrinsic cell apoptosis, indicating the role of GE_4 in embryo implantation and the following epithelial removal. GE_4 interacts with endothelial and Str_2 cells via *Calca* and *Calcrl* in the CALCR signaling pathway (Fig. 5d–f), which plays a key role in human placental development[33]. Among these secreted factors, the levels of *Calca*, *Igf1* and *Lif* gradually increase following the differentiation trajectory, suggesting their expression depends on preimplantation glandular differentiation (Supplementary Fig. 4b–d).

Besides secreted proteins, cells produce bioactive organic compounds as communicating signals between cells. All GE groups are predicted to be the most active senders of bioactive organic compounds among all cell types; the GE_4 group is the most active sender population. Endothelial, stromal, and pericyte cells are among the top receiver groups (Supplementary Fig. 5a, b). All four GE groups exhibit tight communication with uterine stromal cells and endothelial cells (Supplementary Fig. 5c, d). To study the communication between GE_4 and its receivers, we analyzed the compounds released by GE_4 and their targets (Supplementary Fig. 5e). Ornithine is a key substrate for the synthesis of proline, polyamines, and citrulline. Decarboxylation of ornithine plays a role in embryo development during the periimplantation period of pregnancy in sheep[34]. GE_4 cells send ornithine to pericytes. GE_4 cells also send L-glutamine to stromal cells, which improves preimplantation human and mouse embryo development[35,36] and alleviates intrauterine growth restriction[37]. The GE_4 group sends spermine to luminal epithelial cells, a polyamine essential for cell growth and gene expression playing a key role in many mammalian reproductive functions, including implantation and placentation (reviewed in ref. 35). GE_4 cells send lactic acid to stromal cells, which facilitates implantation, decidualization, and fetal growth (reviewed in ref. 38).

These results show all four GE groups communicate with other endometrial cell types involved in periimplantation events by group specific proteins and organic compounds.

https://doi.org/10.1038/s41467-025-57848-w

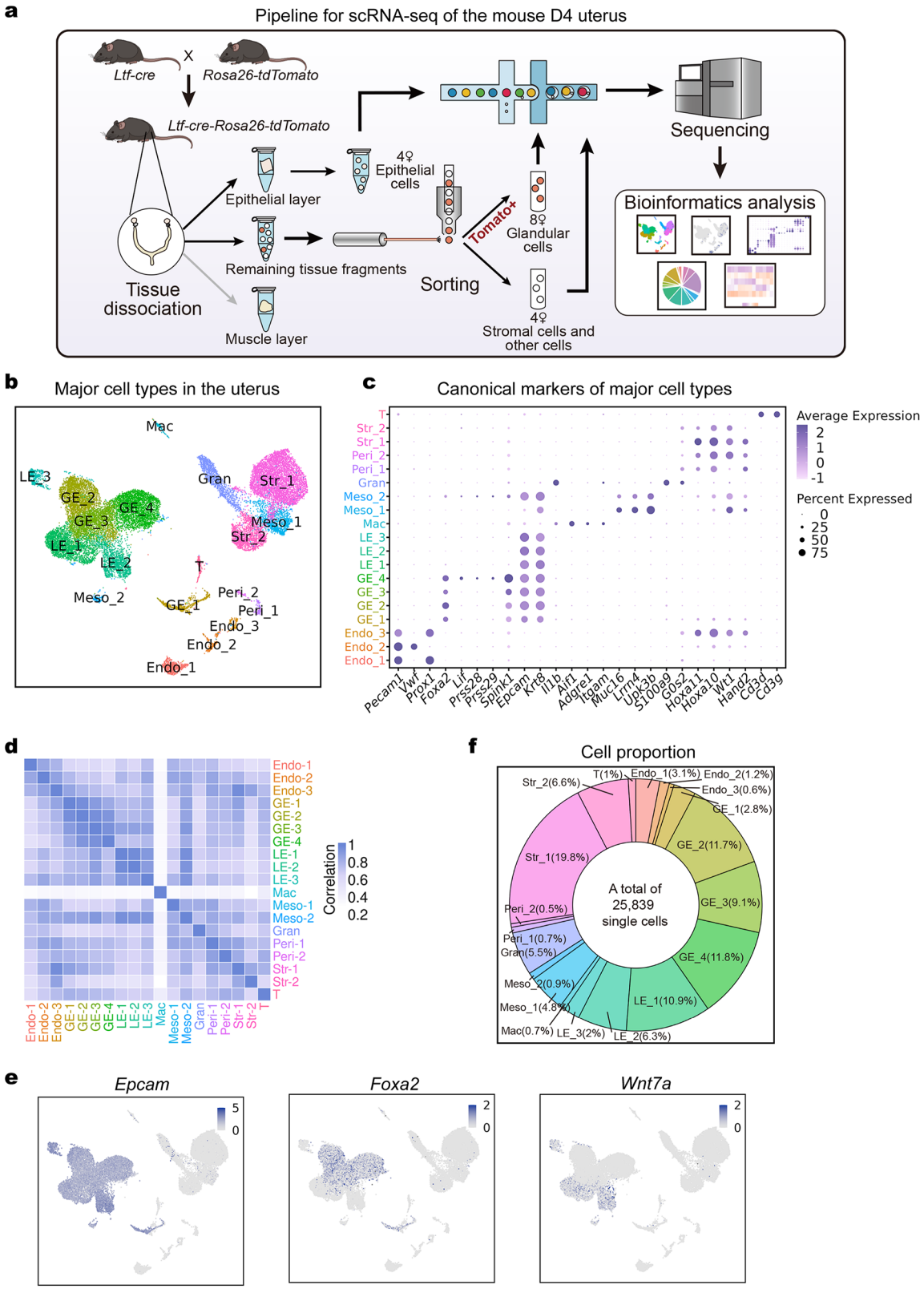


**Fig. 2 | Uterine cells show heterogeneity on day 4 of pregnancy. a** A diagram of the experimental workflow for single-cell transcriptome profiling of mouse uteri on day 4 of pregnancy. Created in BioRender. Li, B. (2025) https://BioRender.com/v89y654. **b** A UMAP of the major cell types in mouse uteri on day 4. **c** The expression of marker genes across different cell types. **d** The Pearson correlation of genes' expression in different cell types. **e** UMAP visualization of the expression of selected marker genes *Epcam*, *Foxa2*, and *Wnt7a* in epithelial cells. **f** A pie chart showing the cell proportions of all cell types in the single-cell analysis. The number of glandular cells is intentionally increased to better investigate subgroups and function of glands.

https://doi.org/10.1038/s41467-025-57848-w


**Fig. 3 | Uterine glandular epithelial cells show heterogeneity on day 4 of pregnancy. a** UMAP visualization of selected marker genes of all glandular cells and different glandular subgroups. **b** A dot plot of marker genes for 4 glandular sub-clusters. Point sizes represent the percents of cell expressing marker genes. **c**, **d** GO and KEGG enrichment analysis of marker genes for different gland cell clusters. The color bar represents the -log10 transformation of enrichment *p*-value. *P*-values were generated by the clusterProfiler using one-sided hypergeometric test without multiple testing correction. **e** Heatmaps of genes in one representative function in each glandular sub-cluster.

https://doi.org/10.1038/s41467-025-57848-w

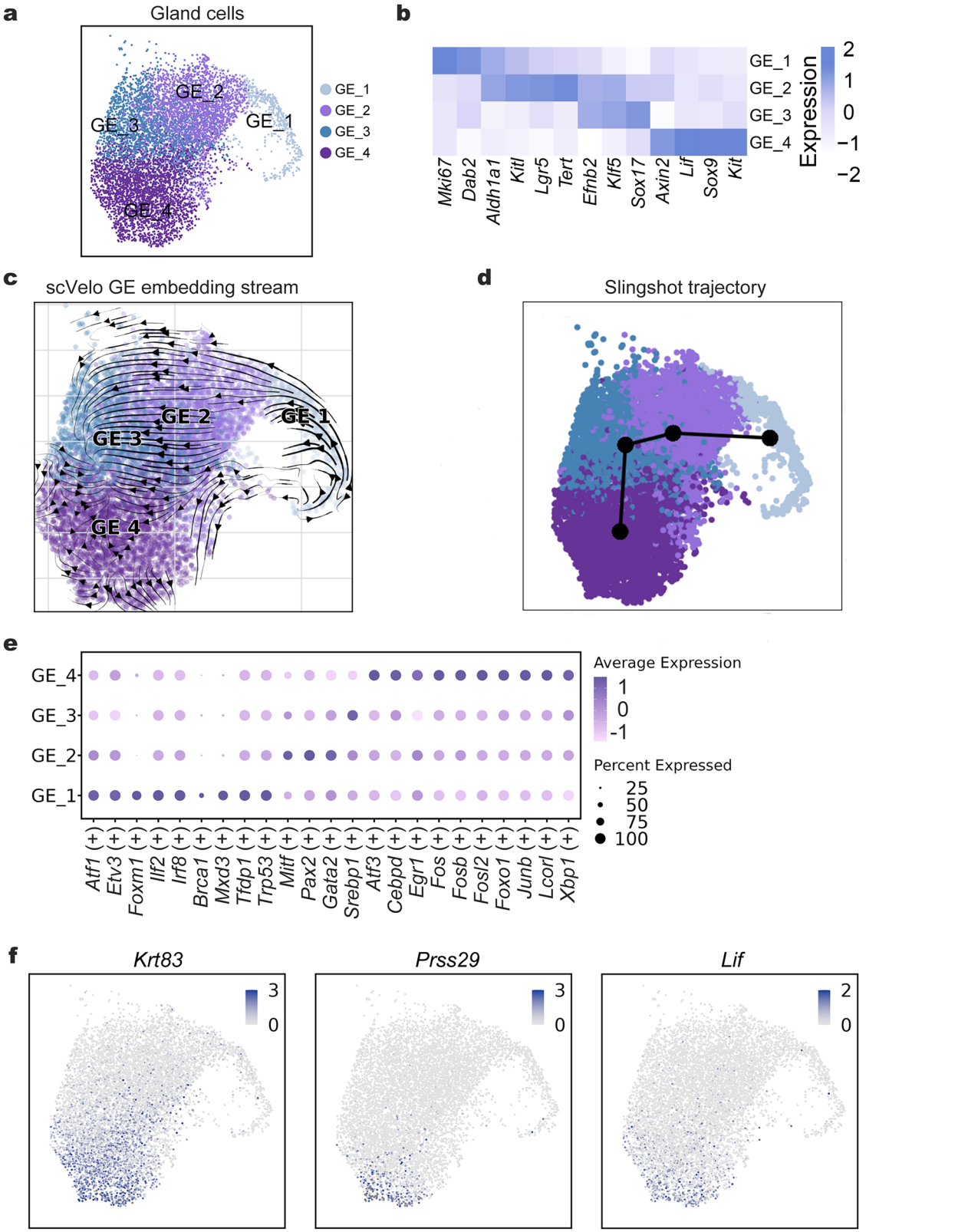


**Fig. 4 | The glandular cell differentiation trajectory. a** UMAP visualization of four different glandular sub-clusters. **b** Heatmap of the feature genes' expression in four different glandular sub-clusters. **c** UMAP visualization of RNA velocity analysis of glandular cells. **d** A Slingshot trajectory of four different glandular sub-clusters. **e** Dot plot of transcription factors active in four different glandular sub-clusters. **f** UMAP visualization of marker genes of GE_4.

## Uterine epithelial deletion of *Foxa2* impairs glandular cell differentiation

The observation of substantially reduced branching of *Foxa2*$^{f/f}$ *Ltf*$^{Cre/+}$ glands, along with the discovery of various GE subtypes, prompts our hypothesis that the abnormal morphology of *Foxa2*$^{f/f}$*Ltf*$^{Cre/+}$ glands is due to a GE differentiation defect. We have shown that GE_4 has the highest protein exporting activity (Fig. 3c–e), and *Lif* positive cells are concentrated in GE_4 at the bottom of the gland pseudo time UMAP

https://doi.org/10.1038/s41467-025-57848-w

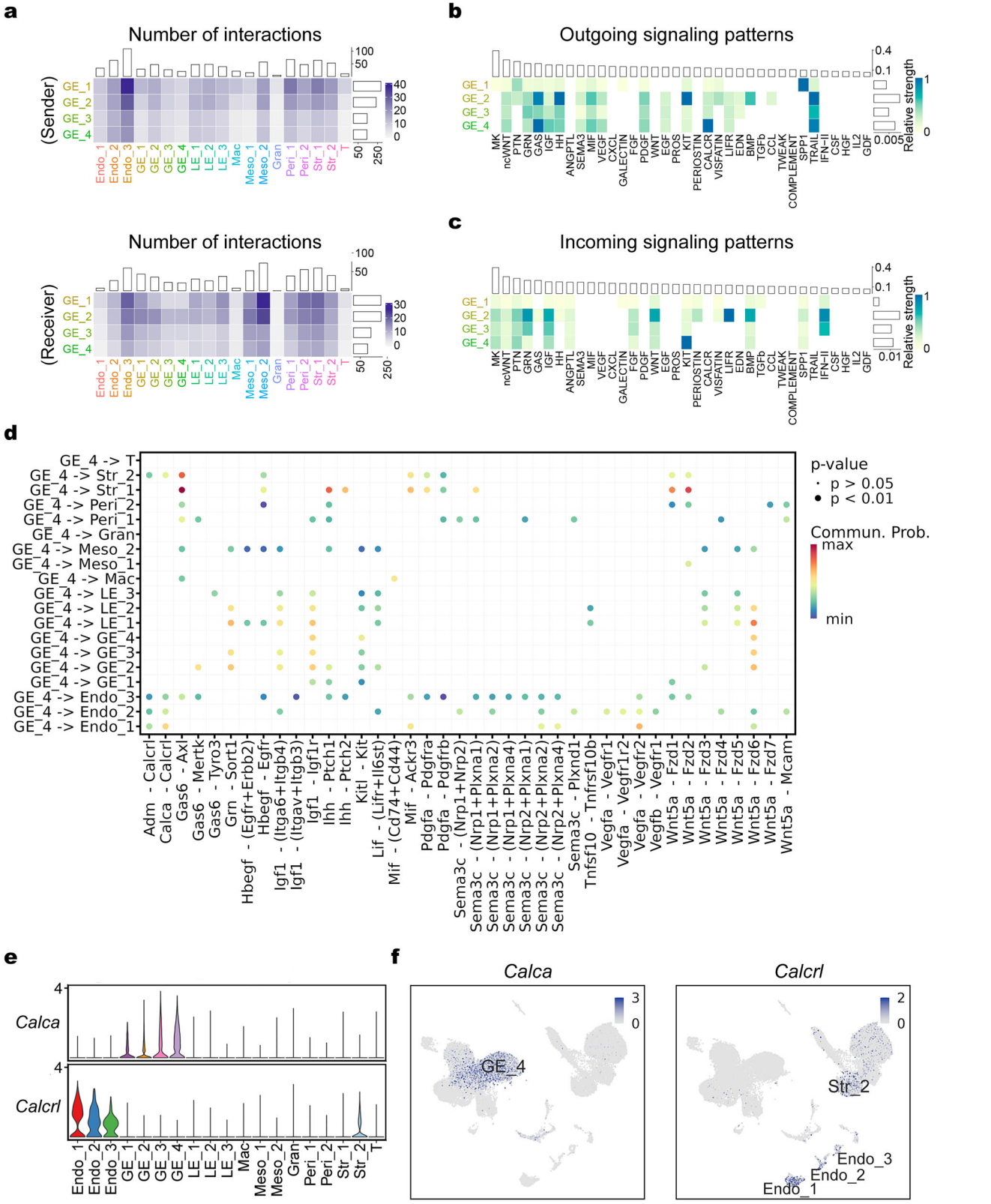


**Fig. 5 | Protein interactions between glandular cells and other uterine cell types. a** Abundance of connections between four glandular sub-clusters and all cell types in day 4 uteri using CellChat. **b**, **c** Heat map showing signals contributing the most to outgoing and incoming signaling of 4 glandular sub-clusters. **d** A dot map showing detailed ligand-receptor pairs from GE_4 to other cell groups. The dot colors and sizes represent the calculated communication probability and *p*-values. *P*-values are computed by a one-sided permutation test. **e** Violin plots showing expression of ligand-receptor pairs of CALCR signal pathway among each cell type in day 4 uterus. **f** UMAP visualization of the expression of CALCR pathway genes *Calca* and *Calcrl*.

https://doi.org/10.1038/s41467-025-57848-w

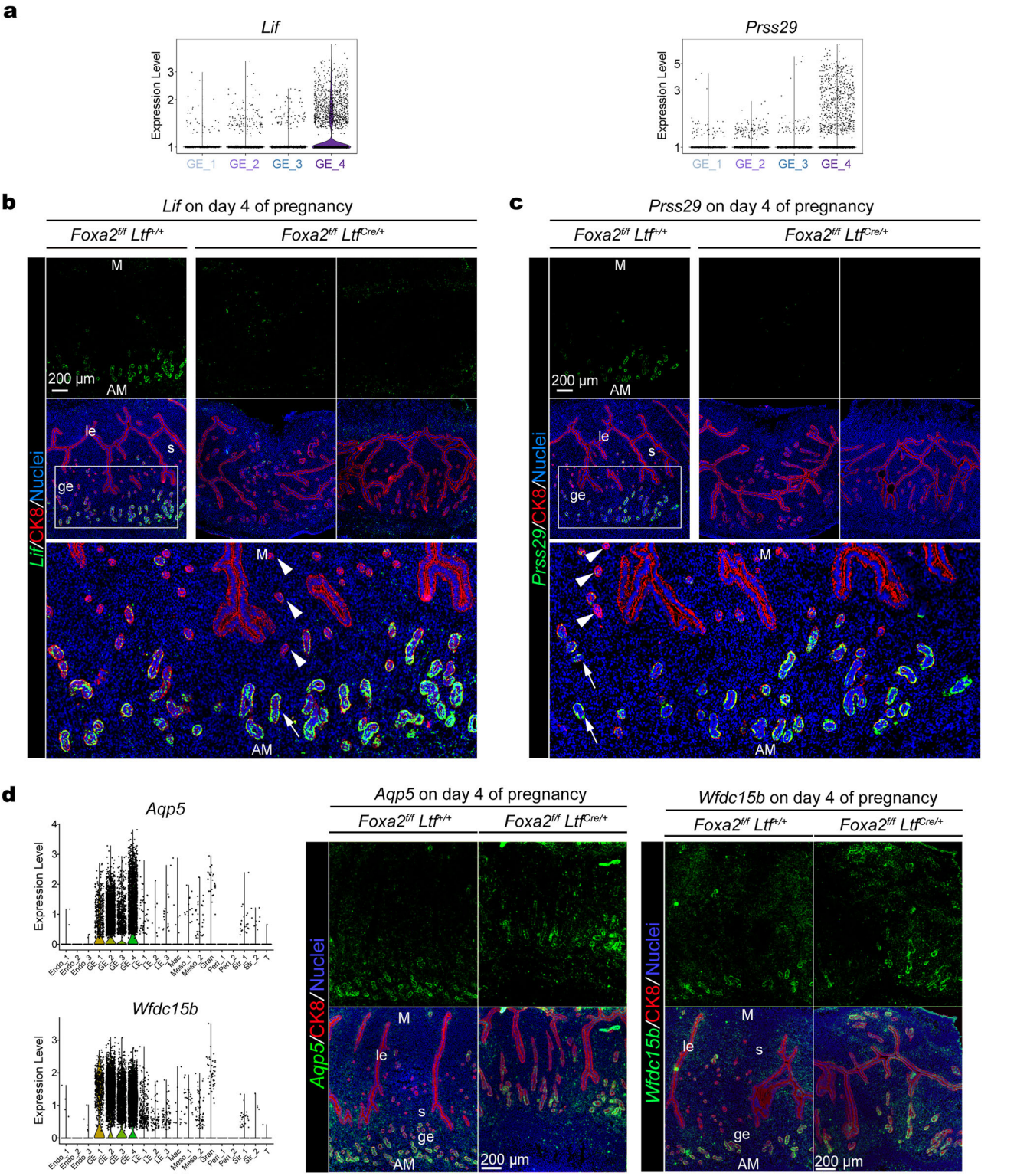


**Fig. 6 | Uterine epithelial deletion of *Foxa2* impairs GE_4 differentiation. a** Violin plots of GE_4 specific markers *Lif* and *Prss29*. **b**, **c** FISH of *Lif* and *Prss29* in *Foxa2*$^{f/f}$ *Ltf*$^{+/+}$ and *Foxa2*$^{f/f}$ *Ltf*$^{Cre/+}$ females on day 4 of pregnancy. Areas within white boxes are presented in a higher magnification. Signals of *Lif* and *Prss29* are detected in glands at the antimesometrial ends (arrows), but not in the glands close to luminal epithelia (arrowheads). Images presented are representative of three independent experiments. **d** Violin plots and FISH of pan-glandular markers *Aqp5* and *Wfdc15b* in *Foxa2*$^{f/f}$ *Ltf*$^{+/+}$ and *Foxa2*$^{f/f}$ *Ltf*$^{Cre/+}$ females on day 4 of pregnancy. Epithelial cells are stained with CK8. Scale bars, 200 μm. le luminal epithelium, ge glandular epithelium, s stroma, M mesometrial pole, AM antimesometrial pole. Images presented are representative of three independent experiments.

(Figs. 4f and 6a). Examination of *Lif* mRNA localization in day 4 frozen sections reveals that *Lif* signals are expressed in *Foxa2*$^{f/f}$*Ltf*$^{+/+}$ GE cells located on the anti-mesometrial side (Fig. 6b). The percentage of *Lif*+ cells among all FOXA2+ cells are quantified in Supplementary Fig. 6. As expected, *Lif* signals are undetectable in *Foxa2*$^{f/f}$ *Ltf*$^{Cre/+}$ uteri (Fig. 6b). Using another newly discovered GE_4 specific gene, *Prss29* (Fig. 6a), we show that *Prss29* signals are only present in *Foxa2*$^{f/f}$*Ltf*$^{+/+}$, but not *Foxa2*$^{f/f}$*Ltf*$^{Cre/+}$, GE cells (Fig. 6c). To demonstrate that *Lif*+ cells are a

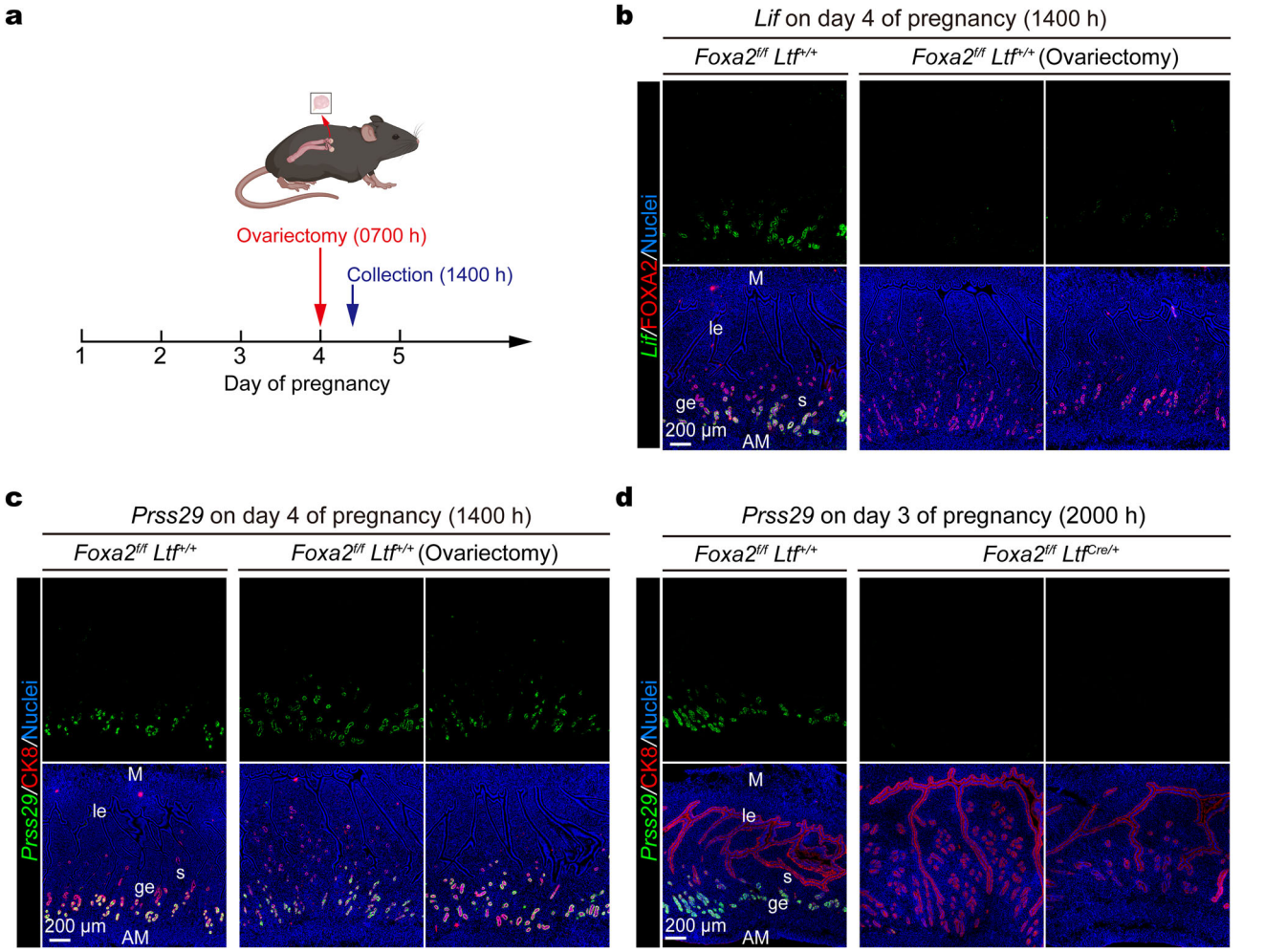


**Fig. 7 | GE_4 differentiation is independent of estrogen secretion on day 4. a.** The scheme of an ovariectomized mouse model for panels b and c. Created in BioRender. Li, B. (2025) https://BioRender.com/v89y654. **b**, **c** FISH of *Lif* and *Prss29* in intact and ovariectomized *Foxa2*$^{f/f}$ *Ltf*$^{+/+}$ females on day 4 of pregnancy. Glandular epithelia are stained with FOXA2. Scale bars, 200 μm. Images presented are representative of three independent experiments. **d** FISH of *Prss29* in *Foxa2*$^{f/f}$ *Ltf*$^{+/+}$ and *Foxa2*$^{f/f}$ *Ltf*$^{Cre/+}$ females in the evening of day 3 of pregnancy. Scale bar, 200 μm. Epithelial cells are stained with CK8. Images presented are representative of three independent experiments. Times of tissue collection are indicated on top of each panel. le, luminal epithelium; ge, glandular epithelium; s, stroma; M, mesometrial pole, AM, antimesometrial pole.

unique population of glandular cells, we examined the expression of *Spink1*. Majority of *Spink1*+ cells do not overlap with Lif+ glandular cells. *Spink1* signals are mainly found on gland stems and are absent in glandular cells located on the anti-mesometrial side (Supplementary Fig. 7). In addition, genes present in all GE cells, including *Aqp5* and *Wfdc15b*, are detectable in both *Foxa2*$^{f/f}$ *Ltf*$^{+/+}$ and *Foxa2*$^{f/f}$*Ltf*$^{Cre/+}$ GE cells (Fig. 6d). Collectively, these results suggest that *Foxa2*$^{f/f}$*Ltf*$^{Cre/+}$ GE cells fail to differentiate into GE_4 cells in the absence of FOXA2, suggesting its critical role in GE differentiation during the preimplantation period.

## FOXA2-mediated gland differentiation is independent of estrogen

Estrogen produced in the morning of day 4 plays a key role in implantation; it also directly regulates LIF production[2,39]. These facts led us to question whether GE_4 is also induced by estrogen secreted on day 4 of pregnancy. To study the effect of this estrogen secretion on GE_4 differentiation, we removed ovaries in the early morning of day 4, which prevents LIF induction and implantation (Fig. 7a, b)[40]. Surprisingly, the GE_4 marker *Prss29* shows a comparable expression pattern in the uteri of intact and ovariectomized *Foxa2*$^{f/f}$ *Ltf*$^{+/+}$ females (Fig. 7c). These results indicate that the GE_4 differentiation is independent of day 4 morning estrogen, although LIF production depends on estrogen. Therefore, it is reasonable to hypothesize that the GE_4 group is specified before the estrogen secretion on the morning of day 4. We examine *Prss29* expression the night before (2000h on day 3). The absence of FOXA2 signals in *Foxa2*$^{f/f}$*Ltf*$^{Cre/+}$ uteri confirmed the complete deletion of FOXA2 in the uteri (Supplementary Fig. 8). Indeed, signals of *Prss29* mRNA are observed in *Foxa2*$^{f/f}$ *Ltf*$^{+/+}$ uteri, but not in *Foxa2*$^{f/f}$ *Ltf*$^{Cre/+}$ uteri (Fig. 7d).

## GE_4 is the functional group for LIF production in response to estrogen stimulation

Our results demonstrate that *Foxa2*$^{f/f}$ *Ltf*$^{Cre/+}$ uteri without GE_4 glandular cells failed to produce LIF. However, it is still unknown whether the GE_4 group is functionally sufficient to produce LIF with estrogen stimulation. In other words, does the emergence of *Prss29*-positive GE_4 cells denote glandular readiness to respond to estrogen? To functionally test the response of glands to estrogen, we stimulated the uterus with estrogen following ovariectomy on various days during the preimplantation period and examined the LIF production after estrogen injections (Fig. 8a). The results show that *Prss29* RNA signals become detectable in glands from day 3 evening (Fig. 8b). Interestingly, uteri with *Prss29* positive cells produce LIF in response to estrogen injection (Fig. 8c). These results demonstrate that Prss29-positive GE_4 is the true

https://doi.org/10.1038/s41467-025-57848-w

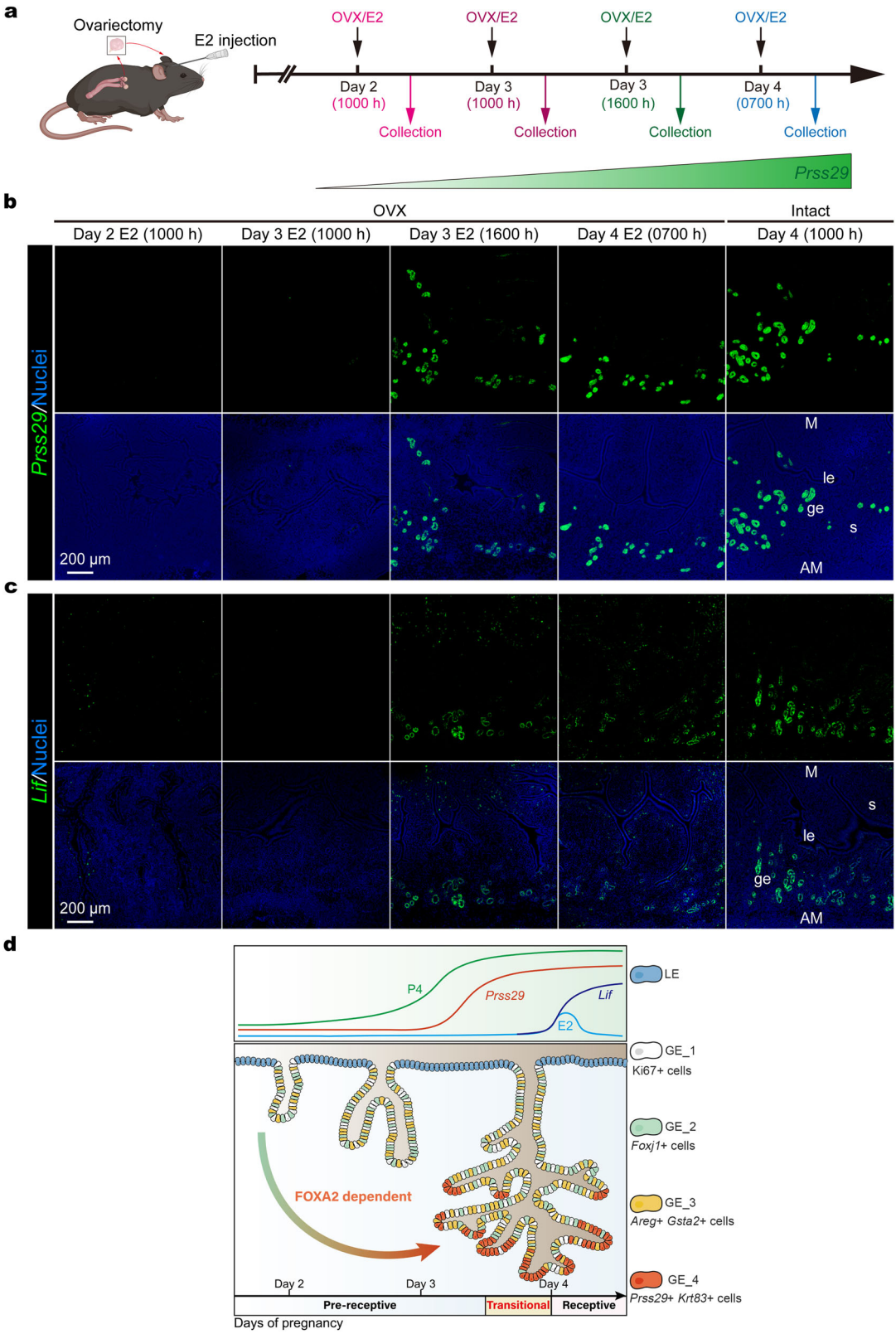


**Fig. 8 | *Prss29* + GE_4 group produces LIF in response to estrogen stimulation.** **a** The scheme of an ovariectomized mouse model used in panels b and c. Created in BioRender. Li, B. (2025) https://BioRender.com/v89y654. **b**, **c** FISH of *Prss29* and *Lif* in ovariectomized wild type females on day 2, 3 and 4 of pregnancy. Uterine tissues collected from intact wild type females at 10am on day 4 of pregnancy serve as positive controls. Scale bars, 200 μm. le luminal epithelium, ge glandular epithelium, s stroma, M mesometrial pole, AM antimesometrial pole. Images presented are representative of three independent experiments. **d** A proposed scheme of FOXA2-mediated glands differentiation in pre-implantation stage. Glands enter transitional phase to acquire the ability to secret LIF in response to estrogen stimulation. Created in BioRender. Li, B. (2025) https://BioRender.com/v89y654.

functional glandular group responsible for LIF production after estrogen stimulation, and that GE_4 differentiation occurs earlier than endogenous estrogen secretion in day 4 morning.

## Discussion

The current study demonstrates that gland cell differentiation, accompanied by glandular morphological changes, is indispensable for successful implantation. Uterine glands develop more branches at the antimesometrial poles from fertilization to the time right before implantation occurs (day 1 to day 4 of pregnancy). At the end of this gland differentiation process, glandular cells are categorized into four groups based on RNA expression profiles. Following a cell developmental order, GE_1 shows high cell proliferative activity; GE_2 further develops and upregulates the ciliated cell marker FOXJ1; GE_3 increases amino acid and lipid metabolism; and GE_4 is active in protein secretion. Notably, LIF, an indispensable growth factor for implantation, is produced exclusively by GE_4 cells, and this group is absent in Foxa2-deficient gland cells. We further demonstrate the GE_4 differentiation is independent of estrogen secretion on day 4 of pregnancy. This group of cells is ready by the evening of day 3 and capable of producing LIF upon estrogen stimulation. A scheme of the glandular differentiation is depicted in Fig. 8d. The identification of a subpopulation of glandular cells responsible for LIF production enhances our understanding of implantation-competent uteri.

The current study reveals the mechanism by which FOXA2 regulates LIF production before implantation. Previous studies showed uterine-specific or epithelial-specific deletion of *Foxa2* causes implantation failure due to LIF deficiency[11]. However, the relationship between FOXA2 and LIF is unknown. Given the transcriptional factor nature of FOXA2, a simple speculation is that FOXA2 regulates *Lif* transcription by binding to the LIF promoter. However, the failure to identify FOXA2 binding peaks close to the LIF promoter region by ChIPseq studies in hepatocytes suggests an alternative explanation[41]. Our current study demonstrates that FOXA2 is critical to glandular differentiation throughout the preimplantation period. *Foxa2* deficiency leads to significantly reduced gland branching and the absence of GE_4 cells. Nevertheless, we cannot completely rule out the possibility that FOXA2 regulates *Lif* transcription as a cis-acting factor. In addition, progesterone is crucial for the secretory activity of uterine glands[19,42]. The role of FOXA2 in glandular differentiation under active progesterone signaling requires further research.

The identification of GE_4 and its markers, such as *Prss29*, enables the prescreening of uterine readiness for estrogen responses. Embryo implantation requires an appropriate crosstalk between a receptive uterus and the competent blastocyst[18]. On day 4 of pregnancy, the uterus becomes receptive after estrogen secretion in the morning. Genes like *Lif*, *Hoxa10*, and *Ihh* have been used to evaluate whether a uterus is in the receptive phase[3]. However, the fact that uterine glands lacking the GE_4 group do not produce LIF, suggests that glandular cell differentiation is indispensable for responding to estrogen and thus initiating implantation. Our study indicates that specific GE_4 markers would be useful in predicting whether the uterus is qualified to enter the receptive phase before estrogen secretion on day 4, which is earlier than the established markers mentioned above.

We quantified the *Lif*+ cells among all FOXA2+ glandular cells (Supplementary Fig. 6). The percentage is higher than that of GE_4 among all gland cells (~30%) in the single-cell analysis. The signal amplification in RNA in situ hybridization tends to spill over to neighboring cells of *Lif*+ cells. We speculate that many Lif-negative GE_1-GE_3 cells are located between GE_4 cells, although our data suggest that GE_4 cells are concentrated in gland branches on the antimesometrial side. In conclusion, the new quantification of Lif+ cells suggests that Lif+ GE_4 cells are a subset of glandular cells.

Our results show that $Foxa2^{f/f}$ $Ltf^{Cre/+}$ glands lack GE_4 group. However, the role of FOXA2 in glandular differentiation remains largely unknow beside its role on GE_4 differentiation. It is possible the differentiation of other gland subgroups is also compromised. While some general glandular epithelial markers are undetectable in $Foxa2^{f/f}$ $Ltf^{Cre/+}$ glands, including *Cxcl15*, some glandular markers including *Aqp5* and *Wfdc15b* remain their expression, suggesting they are independent of FOXA2. More research is needed to comprehensively understand the function of FOXA2 during the preimplantation glandular differentiating process.

It is still unclear whether LIF is the sole important factor secreted by glands critical for pregnancy success. In the glandless mouse model with uterine deficiency of *Foxa2* ($Foxa2^{f/f}$ $Pgr^{cre/+}$), LIF supplementation rescues implantation on day 4 of pregnancy, but cannot support the pregnancy to full term[11], suggesting that glands play additional roles during pregnancy. Previous studies have also shown that uterine glands are critical for fetoplacental development[43]. The current study identified a panel of proteins and metabolites secreted by glands and their interaction with other uterine cell types. More work is needed to address their physiological effects during pregnancy.

*Prss29* is a candidate marker for GE_4 cells on day 4 of pregnancy. *Prss29* is specifically expressed in uterine glands[44]. We show here that $Foxa2^{f/f}$ $Ltf^{Cre/+}$ glands have no *Prss29* expression on day 4 of pregnancy. A previous report also showed that $Foxa2^{f/f}$ $Ltf^{Cre/+}$ uteri have dramatically reduced, or even the expression of *Prss29* is absent on day 5 of pregnancy as compared to $Foxa2^{f/f}$ $Ltf^{Cre/+}$ uteri[11]. Most glandular cells are marked by Prss29-cre when examined 10 days after parturition[44], indicating that most glandular cells possibly differentiate to the GE_4 stage as pregnancy advances, and these cells are not removed after each pregnancy. Therefore, these glandular cells likely undergo a de-differentiation process before the next pregnancy, although it is still not clear when this process starts and ends. These intriguing questions warrant more research.

Our results demonstrate that uterine glands undergo significant morphological changes and cell differentiation in early pregnancy. Previously, our knowledge of uterine gland morphology and function during pregnancy was limited, in contrast with the well-defined morphological and functional changes in mammary glands due to their visual accessibility. At the beginning of pregnancy, mammary glands rapidly proliferate and undergo side branching, and their glandular cells become highly differentiated during lactation[16]. Similarly, our current results show that uterine glands undergo a similar process of extension and differentiation, becoming functionally capable of responding to estrogen before implantation. Our results suggest uterine glands deficient of *Foxa2* fail to develop branches and secrete LIF before implantation. Interestingly, a recent study of $Esr1^{f/f}$ $Pax2^{Cre/+}$ uteri showed a similar branchless glandular structure and failed to secrete LIF in day 4 morning of pregnancy[45]. These observations indicate a strong association between glandular morphology and glandular function. Further research is needed to determine whether glandular structure could be used as a reliable indicator of appropriate glandular development capable of supporting implantation.

Lif-positive GE_4 cells are specifically localized on the antimesometrial side, close to the muscle layer (Fig. 6b). Generally, uterine glandular end-pieces are considered tubular, unlike the alveolar end-pieces in mammary glands or acinar end-pieces in the pancreas[46]. Without whole-mount in situ hybridization experiments, it is uncertain whether GE_4 cells are located in the glandular end-pieces; current research tentatively locates GE_4 cells on uterine cross sections. A recent study of human uterine samples using scRNAseq and spatial RNA profiling showed that ciliated epithelial cells are distributed close to the lumen, while secretory glandular cells are located deep within the stromal cells. The suppression of WNT and activation of Notch signaling promotes differentiation toward the secretory type[47]. Although our study does not observe a significant increase in Notch targets in the GE_4 group, our signaling bioinformatic analysis reveals

an increase of Kit signaling. Determining whether GE_4 cells have specific spatial localization requires further research.

## Methods

### Mice

*Rosa26*$^{tdTomato}$ *Ltf*$^{Cre/+}$ mice were generated by mating *Ltf*$^{cre/+}$ males with *Rosa26-CAG-LSL-Cas9-tdTomato* female mice (C57BL/6J GemPharmatech). *Rosa26*$^{tdTomato}$ *Ltf*$^{Cre/+}$ mice were housed in the model animal research center of Shandong University with a controlled environment (20–26 °C, 40–70% humidity, 12-h light/dark cycle, lights on at 7 AM). All animal experiments procedures were approved by the Institutional Animal Care and Use Committee of Shandong University.

*Foxa2*$^{f/f}$ mice[48] were originally obtained from Jeff Whitsett's lab at our Institute. *Foxa2*$^{f/f}$ *Ltf*$^{Cre/+}$ mice were generated by mating *Foxa2*$^{f/f}$ females with *Ltf*$^{Cre/+}$ males[17] (C57BL/6 and albino B6 mixed background). *Foxa2*$^{f/f}$ and *Foxa2*$^{f/f}$ *Ltf*$^{Cre/+}$ mice were housed in the animal care facility at Cincinnati Children's Hospital Medical Center according to the National Institute of Health and institutional guidelines for laboratory animals. All protocols were approved by the Cincinnati Children's Animal Care and Use Committee. Mice were provided with irradiated Laboratory Rodent Diet 5R53 and autoclaved water ad libitum. These mice were housed under a 12:12 h light:dark cycle with controlled ambient temperature and humidity. At least three mice, aged between 2 and 5 months, from each genotype were used for each individual experiment.

### Analysis of pregnancy events

Adult females between 2 and 4 months old from each genotype were randomly chosen and housed overnight with a fertile male; the morning of finding a vaginal plug was considered successful mating (day 1 of pregnancy). WT and mutant plug-positive females were then housed separately until processing for experiments.

### Fluorescence In Situ Hybridization (FISH)

FISH experiments were performed as previously described[13]. Briefly, frozen sections (12 μm) were processed on the same slide for each probe. Following fixation (in 4% paraformaldehyde) and acetylation, slides were hybridized at 55 °C with digoxigenin-labeled *Lif, Prss29, Aqp5, Wfdc15b or Spink1* probes. Anti-DIG-peroxidase was applied onto hybridized slides following washing and peroxide quenching. The color was developed by TSA (Tyramide Signal Amplification) fluorescein according to the manufacturer's instructions (PerkinElmer). Epithelia were stained using a CK8 antibody (1:300, TROMA-I, Hybridoma Bank, Iowa). Glands were stained using a FOXA2 antibody (1:300, 8186s, Cell Signaling Technology). Images were captured using a confocal microscope (Nikon Eclipse TE2000). Nuclei staining was performed using Hoechst 33342 (4 μg/ml, H1399, Thermo Scientific).

### Whole-mount immunostaining for 3D imaging

Whole-mount immunostaining with 3DISCO tissue clearing was performed as previously described[15]. Briefly, uterine samples were fixed in Dent's Fixative (Methanol:DMSO (4:1)) overnight in −20 °C and then washed with 100% methanol for three times. The samples were bleached with 3% $H_2O_2$ in methanol at 4 °C overnight to remove pigmentation. After washing in 1% PBS-T for 6 times with 1 h each, samples were incubated with E-cadherin antibody (1:200, 3195 s, Cell Signaling Technology) at 4 °C on a rotor for 7 days. After incubation, the samples were washed with 1% PBS-T six times for 1 hour each and incubated with Alexa-conjugated 594 antibody (1:200, Jackson Immuno Research) in a light-proof box for 4 days at 4 °C. After six washes in 1% PBS-T at room temperature, samples were dehydrated in 100% methanol for 1 h and then cleared in benzyl alcohol/benzyl benzoate (BABB) solution for at least 1 h in a light-proof box.

### 3D imaging and processing

3D pictures were acquired using a Nikon FN1 Upright Microscope. Samples were laid on slides, covered with BABB, and enclosed by cover slips for confocal imaging using a 10X objective with 8 μm Z-stack. All files were generated by Nikon elements and were imported into Imaris (version 10.1, Bitplane) for visualization and 3D reconstruction. To obtain the 3D structure of the tissue, the surface tool was utilized. To isolate a specific region of the tissue, the surface tool was manually used to segment the images, and the mask option was selected for subsequent pseudo-coloring. 3D images were generated using the snapshot tool.

### Glandular branch analysis

The 3D uterine epithelial structures were used to count glandular branches. Segmentation of glands from the uterine lumen was completed using Imaris. Detailed segmentation steps with parameters are included in supplementary methods. All connected glandular cells that share a single connection point with the uterine lumen are defined as one gland. Selected individual glands are presented in Fig. 1a. A schematic representation of the definition of gland branches is depicted in Fig. 1b. Any glands in which the gland cavity has no bifurcation are defined as "0 branch" glands. Glands with one bifurcation point in the cavity are referred to as "1 branch" glands. Glands with more than one bifurcation point in the gland cavity are classified as ">1 branch" glands. Branches with a length equal to or shorter than their width are excluded. To count glands, all glands in a uterine region with a length of no less than 1 mm are included. In each pregnancy date group or genotype, three uterine horns from different females are used for gland counting.

### Single-cell RNA sequencing of day 4 mouse uteri

*Rosa26*$^{tdTomato}$ *Ltf*$^{Cre/+}$ females were mated with fertile males (C57BL/6 background). Pregnancy was confirmed on day 4 by recovering blastocysts from the uterus. Uterine tissues were collected from animals at 11:00am on day 4 of pregnancy. The uteri were cut into 2–3 mm fragments and were digested in 62.5 mg/ml pancreatin (Sigma, P3292) and 30 mg/ml dispase (Roche, 4942078001) at 37 °C for 1 h. Subsequently, the luminal epithelial layer was carefully separated from other uterine tissues under a stereomicroscope by a gentle squeeze using a pair of blunt forceps. Luminal epithelial sheets were rinsed in 1× PBS and further digested in Accumax solution (Sigma-Aldrich, A7089) at 37 °C for 30 min with agitation until the epithelial layer was digested into a single cell suspension. Cell suspension was filtered through a 70 μm cell strainer. The single cell suspension of luminal epithelial cells from 4 females was kept for single cell sequencing analysis. The remaining uterine tissues without luminal epithelia were subjected to Accumax digestion at 37 °C for 30 min, and the resulting cell suspension was filtered through a 70 μm cell strainer to remove cell debris and the muscle layer. The cells were centrifuged at 400 × *g* for 10 minutes and resuspended in 2% FBS. To label dead cells, cells were incubated with dead cell stain SYTOX green (Thermo Fisher, S7020) for 15 min at 4 °C. Using a CytoFlex SRT Cell Sorter (Beckman Coulter), glandular epithelial cells (tdTomato positive and FITC negative cells) were sorted from the single cell suspension of 8 females, and the rest endometrial cells (tdTomato negative and FITC negative cells) were sorted from the single cell suspension of 4 females. The samples of luminal epithelial, glandular epithelial and other endometrial cells were then loaded to 10X Chromium to capture single cell according to the manufacturer's instructions of 10X Genomics Chromium Single-Cell 3′ kit (V3). Subsequent cDNA amplification and library construction steps were performed according to the standard protocol. Single-cell libraries were sequenced on Illumina NovaSeq 6000 sequencing system using 150 bp paired-end sequencing.

### Single-cell RNA sequencing data processing

Raw data of bcl files from the NovaSeq 6000 system were converted to fastq files using the Illumina bcl2fastq software. And the fastq files were aligned to the GRCm38 mouse reference genome using the CellRanger software (version 3.1.0). The standard workflow of cell clustering in Seurat (version 5.0.1) was utilized. Cells with fewer than 200 detected genes or the total mitochondrial gene expression exceeding 20% were removed. Genes expressed in fewer than 3 cells were removed. After filtering, the remaining cells were kept for downstream analysis. To remove the batch effect between different samples, harmony R package was used. The UMAP algorithm was used as the preferred dimensional reduction method. A total of 2000 highly variable genes were selected using the FindVariableFeatures function, and then the top 50 PCs were calculated using the runPCA function. By using FindNeighbors, FindClusters and RunUMAP function, 19 major cell clusters were identified and annotated based on the well-known marker genes. Endothelial cell markers included: *Pecam1*, *Vwf*, *Prox1*. Glandular epithelial cell markers included: *Foxa2*, *Cxcl15*, *Prss28*, *Prss29*, *Spink1*. Luminal epithelial cell markers included: *Epcam*, *Krt8*. Macrophage markers included: *Il1b*, *Aif1*, *Adgre1*, *Itgam1*. Mesothelial cell markers included: *Muc16*, *Lrrn4*, *Upk3b*. Stromal cell markers included: *Hoxa11*, *Hoxa10*, *Wt1*, *Hand2*. T cell markers included: *Cd3d*, *Cd3g*. To identify differentially expressed genes among 4 glandular epithelial clusters, the FindMarkers function with the Wilcoxon rank-sum test algorithm was used under the following criteria: logfc. threshold >0.25, min.pct >0.25.

### Constructing cell pseudotime trajectories

Slingshot R package (version 2.6.0) was used to generate the pseudotime trajectory of glandular epithelial cell sub-clusters. Using Slingshot function, we identified the global lineage structure with a cluster-based minimum spanning tree (MST) and fitted simultaneous principal curves to describe each lineage.

### Functional enrichment analysis

Gene Ontology (GO) analysis and Kyoto Encyclopedia of Genes and Genomes (KEGG) analysis were performed using clusterProfiler (version 4.10.0) R package. The terms with $p$ value < 0.05 were selected.

### CellChat

To identify and compare cell-cell interactions, we used CellChat (version 1.6.1) R package for further analysis. We followed the standard workflow, using identifyOverExpressedGenes function to get the overexpressed genes and computeCommunProb function to get the potential intercellular communication. To remove the potential artifact due to unproportional cell populations, the population.size parameter in the computeCommunProb function was set to TRUE.

### MEBOCOST

The inference of metabolites mediated cell-cell communication between glandular epithelial cell sub-clusters and other cell clusters was performed using MEBOCOST python package (version 1.0.2). We transformed the Seurat object to Scanpy object and followed the standard MEBOCOST workflow (https://github.com/zhengrongbin/MEBOCOST).

### Transcriptional regulation analysis of glandular epithelial cell clusters

In order to analyze the underlying transcription factors and their target genes which regulate glandular epithelial cell differentiation, we used pySCENIC (version 0.12.1) python package to access the activity of these genes in individual cells. Co-expression modules were inferred by grnboost2 function. The indirect targets from these modules were pruned using cis regulatory motif discovery. Aucell function was used to quantify the activity of these transcription factors and their target genes by enrichment scores.

### Correlation analysis

Using the AverageExpression function in the Seurat package, we calculated the average expression levels of the transcriptome for each cell type, followed by the calculation of the Pearson correlation coefficient between all cell clusters.

### RNA velocity analysis

Read annotations for gland epithelial cells were performed using the alevin-fry (version 0.8.2) command-line tool with fastq and splici reference files. Alevin-fry is an accurate and computationally efficient tool for preprocessing scRNA-seq data for RNA velocity analysis. The splici reference file was created using the pyroe python package based on the GRCm38 mouse reference genome. The genome annotations GRCm38 references were used to count molecules while separating them into two categories: 'spliced' or 'unspliced'. After the alevin-fry workflow with default parameters, 7743 high-quality gland epithelial cells with spliced and unspliced reads were obtained and used to analyze the velocities. The RNA velocities were calculated using scVelo (version 0.2.5) python package. Finally, The RNA velocity vectors were embedded to the UMAP plot produced by the Seurat R package.

### Immunostaining

Staining for FOXA2 (Cell Signaling Technology, 8186S), CK8 (TROMA-1, Hybridoma Bank, Iowa), Tomato (Chromotek, 5f8) was performed using secondary antibodies conjugated with Alexa 488, Alexa 594 or biotin (Jackson Immuno Research). Nuclear staining was performed using Hoechst 33342 (4 µg/ml, H1399, Thermo Scientific). Tissue sections from control and experimental groups were processed on the same slide for each experiment. Images presented are representative of three independent experiments.

### Statistical analysis

Statistical analyses were conducted using GraphPad Prism (v6.0) and R (v4.2.2) along with RStudio (2023.12.0). Each experiment was repeated at least three times. Data are shown as mean ± SEM. Statistical analyses were performed using a two-tailed Student's $t$ test and Wilcoxon rank-sum test or *Chi*-square test. A $P$ value less than 0.05 was considered statistically significant.

### Reporting summary

Further information on research design is available in the Nature Portfolio Reporting Summary linked to this article.

## Data availability

The raw and processed scRNA-seq data generated in this study have been deposited in the NCBI Gene Expression Omnibus (GEO) under accession number GSE275806. The processed datasets, including RDS files, are available for download there. Source data are provided with this paper.

## Code availability

Codes used in this study are deposited at Zenodo [https://doi.org/10.5281/zenodo.14874123].

## References

1. Wang, H. & Dey, S. K. Roadmap to embryo implantation: clues from mouse models. *Nat. Rev.* **7**, 185–199 (2006).
2. Dey, S. K. et al. Molecular cues to implantation. *Endocr. Rev.* **25**, 341–373 (2004).
3. Paria, B. C., Reese, J., Das, S. K. & Dey, S. K. Deciphering the cross-talk of implantation: advances and challenges. *Science* **296**, 2185–2188 (2002).

4. Stewart, C. L. et al. Blastocyst implantation depends on maternal expression of leukaemia inhibitory factor. *Nature* **359**, 76–79 (1992).
5. Song, H., Lim, H., Das, S. K., Paria, B. C. & Dey, S. K. Dysregulation of EGF family of growth factors and COX-2 in the uterus during the preattachment and attachment reactions of the blastocyst with the luminal epithelium correlates with implantation failure in LIF-deficient mice. *Mol. Endocrinol.* **14**, 1147–1161 (2000).
6. Sherwin, J. R. et al. Identification of genes regulated by leukemia-inhibitory factor in the mouse uterus at the time of implantation. *Mol. Endocrinol.* **18**, 2185–2195 (2004).
7. Cullinan, E. B. et al. Leukemia inhibitory factor (LIF) and LIF receptor expression in human endometrium suggests a potential autocrine/paracrine function in regulating embryo implantation. *Proc. Natl Acad. Sci. USA* **93**, 3115–3120 (1996).
8. Lass, A., Weiser, W., Munafo, A. & Loumaye, E. Leukemia inhibitory factor in human reproduction. *Fertil. Steril.* **76**, 1091–1096 (2001).
9. Golson, M. L. & Kaestner, K. H. Fox transcription factors: from development to disease. *Development* **143**, 4558–4570 (2016).
10. Kelleher, A. M. et al. Integrative analysis of the forkhead box A2 (FOXA2) cistrome for the human endometrium. *FASEB J.* **33**, 8543–8554 (2019).
11. Kelleher, A. M. et al. Forkhead box a2 (FOXA2) is essential for uterine function and fertility. *Proc. Natl Acad. Sci. USA* **114**, E1018–E1026 (2017).
12. Jeong, J. W. et al. Foxa2 is essential for mouse endometrial gland development and fertility. *Biol. Reprod.* **83**, 396–403 (2010).
13. Matsuo, M. et al. Targeted depletion of uterine glandular Foxa2 induces embryonic diapause in mice. *Elife* **11**, e78277 (2022).
14. Cooke, P. S., Spencer, T. E., Bartol, F. F. & Hayashi, K. Uterine glands: development, function and experimental model systems. *Mol. Hum. Reprod.* **19**, 547–558 (2013).
15. Yuan, J. et al. Tridimensional visualization reveals direct communication between the embryo and glands critical for implantation. *Nat. Commun.* **9**, 603 (2018).
16. Macias, H. & Hinck, L. Mammary gland development. *Wiley Interdiscip. Rev. Dev. Biol.* **1**, 533–557 (2012).
17. Daikoku, T. et al. Lactoferrin-iCre: a new mouse line to study uterine epithelial gene function. *Endocrinology* **155**, 2718–2724 (2014).
18. Cha, J., Sun, X. & Dey, S. K. Mechanisms of implantation: strategies for successful pregnancy. *Nat. Med.* **18**, 1754–1767 (2012).
19. Kelleher, A. M., DeMayo, F. J. & Spencer, T. E. Uterine Glands: Developmental Biology and Functional Roles in Pregnancy. *Endocr. Rev.* **40**, 1424–1445 (2019).
20. Li, R. et al. TRIM28 modulates nuclear receptor signaling to regulate uterine function. *Nat. Commun.* **14**, 4605 (2023).
21. Stadhouders, R., Filion, G. J. & Graf, T. Transcription factors and 3D genome conformation in cell-fate decisions. *Nature* **569**, 345–354 (2019).
22. Katoh, M. & Katoh, M. Human FOX gene family (Review). *Int J. Oncol.* **25**, 1495–1500 (2004).
23. Barisone, G. A., Yun, J. S. & Diaz, E. From cerebellar proliferation to tumorigenesis: new insights into the role of Mad3. *Cell cycle* **7**, 423–427 (2008).
24. Hilakivi-Clarke, L. Estrogens, BRCA1, and breast cancer. *Cancer Res.* **60**, 4993–5001 (2000).
25. Rubel, C. A. et al. A Gata2-Dependent Transcription Network Regulates Uterine Progesterone Responsiveness and Endometrial Function. *Cell Rep.* **17**, 1414–1425 (2016).
26. Horton, J. D., Goldstein, J. L. & Brown, M. S. SREBPs: activators of the complete program of cholesterol and fatty acid synthesis in the liver. *J. Clin. Investig.* **109**, 1125–1131 (2002).
27. Vasquez, Y. M. et al. FOXO1 regulates uterine epithelial integrity and progesterone receptor expression critical for embryo implantation. *PLoS Genet* **14**, e1007787 (2018).
28. Adiguzel, D. & Celik-Ozenci, C. FoxO1 is a cell-specific core transcription factor for endometrial remodeling and homeostasis during menstrual cycle and early pregnancy. *Hum. Reprod. update* **27**, 570–583 (2021).
29. Rotem, I. et al. Osteopontin promotes infarct repair. *Basic Res Cardiol.* **117**, 51 (2022).
30. Yasuda, A. et al. The stem cell factor/c-kit receptor pathway enhances proliferation and invasion of pancreatic cancer cells. *Mol. Cancer* **5**, 46 (2006).
31. Jia, Y., Wang, Y. & Xie, J. The Hedgehog pathway: role in cell differentiation, polarity and proliferation. *Arch. Toxicol.* **89**, 179–191 (2015).
32. Xu, C., Zhu, S., Wu, M., Han, W. & Yu, Y. Functional receptors and intracellular signal pathways of midkine (MK) and pleiotrophin (PTN). *Biol. Pharm. Bull.* **37**, 511–520 (2014).
33. Dong, Y. L. et al. Calcitonin gene-related peptide (CALCA) is a proangiogenic growth factor in the human placental development. *Biol. Reprod.* **76**, 892–899 (2007).
34. Lenis, Y. Y. et al. Functional roles of ornithine decarboxylase and arginine decarboxylase during the peri-implantation period of pregnancy in sheep. *J. Anim. Sci. Biotechnol.* **9**, 10 (2018).
35. Devreker, F., Winston, R. M. & Hardy, K. Glutamine improves human preimplantation development in vitro. *Fertil. Steril.* **69**, 293–299 (1998).
36. Rezk, Y., Huff, C. & Rizk, B. Effect of glutamine on preimplantation mouse embryo development in vitro. *Am. J. Obstet. Gynecol.* **190**, 1450–1454 (2004).
37. Zhu, Y. et al. Maternal L-glutamine supplementation during late gestation alleviates intrauterine growth restriction-induced intestinal dysfunction in piglets. *Amino Acids* **50**, 1289–1299 (2018).
38. Ma, L. N., Huang, X. B., Muyayalo, K. P., Mor, G. & Liao, A. H. Lactic Acid: A Novel Signaling Molecule in Early Pregnancy? *Front Immunol.* **11**, 279 (2020).
39. Ma, W. G., Song, H., Das, S. K., Paria, B. C. & Dey, S. K. Estrogen is a critical determinant that specifies the duration of the window of uterine receptivity for implantation. *Proc. Natl Acad. Sci. USA* **100**, 2963–2968 (2003).
40. Rosario, G. X. & Stewart, C. L. The Multifaceted Actions of Leukaemia Inhibitory Factor in Mediating Uterine Receptivity and Embryo Implantation. *Am. J. Reprod. Immunol.* **75**, 246–255 (2016).
41. Li, Z., Tuteja, G., Schug, J. & Kaestner, K. H. Foxa1 and Foxa2 are essential for sexual dimorphism in liver cancer. *Cell* **148**, 72–83 (2012).
42. Spencer, T. E. Biological roles of uterine glands in pregnancy. *Semin Reprod. Med.* **32**, 346–357 (2014).
43. Dhakal, P., Kelleher, A. M., Behura, S. K. & Spencer, T. E. Sexually dimorphic effects of forkhead box a2 (FOXA2) and uterine glands on decidualization and fetoplacental development. *Proc. Natl Acad. Sci. USA* **117**, 23952–23959 (2020).
44. Kelleher, A. M., Allen, C. C., Davis, D. J. & Spencer, T. E. Prss29 Cre recombinase mice are useful to study adult uterine gland function. *Genesis* **60**, e23493 (2022).
45. Granger, K. et al. Murine uterine gland branching is necessary for gland function in implantation. *Mol. Hum. Reprod.* **30**, gaae020 (2024).
46. Khan, S., Fitch, S., Knox, S. & Arora, R. Exocrine gland structure-function relationships. *Development* **149**, dev197657 (2022).
47. Garcia-Alonso, L. et al. Mapping the temporal and spatial dynamics of the human endometrium in vivo and in vitro. *Nat. Genet* **53**, 1698–1711 (2021).
48. Sund, N. J. et al. Hepatocyte nuclear factor 3beta (Foxa2) is dispensable for maintaining the differentiated state of the adult hepatocyte. *Mol. Cell. Biol.* **20**, 5175–5183 (2000).

## Acknowledgements
We sincerely thank Katie Gerhardt for her efficient editing of the manuscript. We thank Yan Zhang and Limei Wang for their assistance with fluorescence-activated cell sorting at the Translational Medicine Core Facility of Advanced Medical Research Institute in Shandong University. This work was supported in part by the national key research and development program of China (2022YFC2702400 to J.Y.), the national natural science foundation of China (grant 32270906 to J.Y.), the natural science foundation of Shandong province (grant 2022HWYQ-054 to J.Y.), and NIH grants HD068524 (X.S. and S.K.D.) and HD103475 (S.K.D.). Bo Li is supported by a Lalor foundation postdoctoral fellowship.

## Author contributions
S.K.D., J.Y. and X.S. designed research; Z.J., B.L., J.Y., M.M., A.D. and A.M. performed research; Z.J., B.L., M.M., J.Y. and X.S. analyzed data; and B.L., S.K.D., J.Y. and X.S. wrote the paper.

## Competing interests
The authors declare no competing interests.

## Additional information
**Supplementary information** The online version contains supplementary material available at https://doi.org/10.1038/s41467-025-57848-w.

**Correspondence** and requests for materials should be addressed to Sudhansu K. Dey, Jia Yuan or Xiaofei Sun.

**Peer review information** *Nature Communications* thanks the anonymous reviewers for their contribution to the peer review of this work. A peer review file is available.